Research Article | Vol. 27, No. 16 | 5 Aug 2019 | OPTICS EXPRESS 22960
Optics EXPRESS

Self referencing attosecond interferometer with zeptosecond precision

JAN TROSS,[1] GEORGIOS KOLLIOPOULOS,[1,2] AND CARLOS A. TRALLERO-HERRERO[1,3,*]

[1]*J.R. Macdonald Laboratory, Department of Physics, Kansas State University, Manhattan, Kansas 66506, USA*
[2]*Extreme Light Infrastructure - Nuclear Physics, Romania*
[3]*Department of Physics, University of Connecticut, Storrs, CT 06268, USA*
[*]*carlos.trallero@uconn.edu*

Abstract: In this work we demonstrate the generation of two intense, ultrafast laser pulses that allow a controlled interferometric measurement of higher harmonic generation pulses with 12.8 attoseconds in resolution (half the atomic unit of time) and a precision as low as 680 zeptoseconds (10^{-21} seconds). We create two replicas of a driving femtosecond pulse which share the same optical path except at the focus where they converge to two foci. An attosecond pulse train emerges from each focus through the process of high harmonic generation. The two attosecond pulse trains from each focus interfere in the far field producing a clear interference pattern in the extreme ultraviolet region. By controlling the relative optical phase (carrier envelope phase for pulsed fields) between the two driving laser pulses we are able to actively influence the delay between the pulses and are able to perform very stable and precise pump-probe experiments. Because of the phase shaping operation occurs homogeneously across the entire spatial profile, we effectively create two indistinguishable intense laser pulses or a common path interferometer for attosecond pulses. Commonality across the two beams means that they are extremely stable to environmental and mechanical fluctuations up to a Rayleigh range from the focus. In our opinion this represents an ideal source for homodyne and heterodyne spectroscopic measurements with sub-attosecond precision.

© 2019 Optical Society of America under the terms of the OSA Open Access Publishing Agreement

1. Introduction

It takes photons, carrying information about the electromagnetic interaction between electrons and atoms about 0.5 attoseconds to travel across one carbon atom. This makes attoseconds the natural time scale for bound electrons in atoms, molecules and solids. For this reason attosecond metrology has been at the forefront of the optical sciences for the last fifteen years [1–10] and it represents the latest time-domain frontier of the quantum world [11]. Attosecond light pulses are commonly generated using higher-order harmonic generation (HHG) [12, 13], a process capable of generating extreme ultraviolet (XUV) coherent pulses [14–16]. In addition to generating attosecond pulses, HHG can be used to study the structure and dynamics of atoms and molecules by looking at the spectral content of the XUV spectrum. This approach is known as HHG spectroscopy and it provides a coherent, time-dependent approach to studying structure and dynamics in the quantum world [17, 18]. To explore the coherent nature of the method [19], several approaches have been used [2, 20–24] and in this article we will focus mainly on the two-source interferometry method, first proposed in [25] by Zerne et al. We will demonstrate how our technique is improving the ability to tune the interferometer, while still maintaining sub-attosecond stability. Our method is an alternative approach to the method presented in [26–28], which had some recent applications [29, 30]. Noteworthy here is a recent publication [27] where a common path interferometer has been built using birefringent wedges on a translation stage. As both laser pulses travel on the same beam path and share the same

#367363 https://doi.org/10.1364/OE.27.022960
Journal © 2019 Received 13 May 2019; revised 15 Jul 2019; accepted 16 Jul 2019; published 26 Jul 2019

Optics EXPRESS

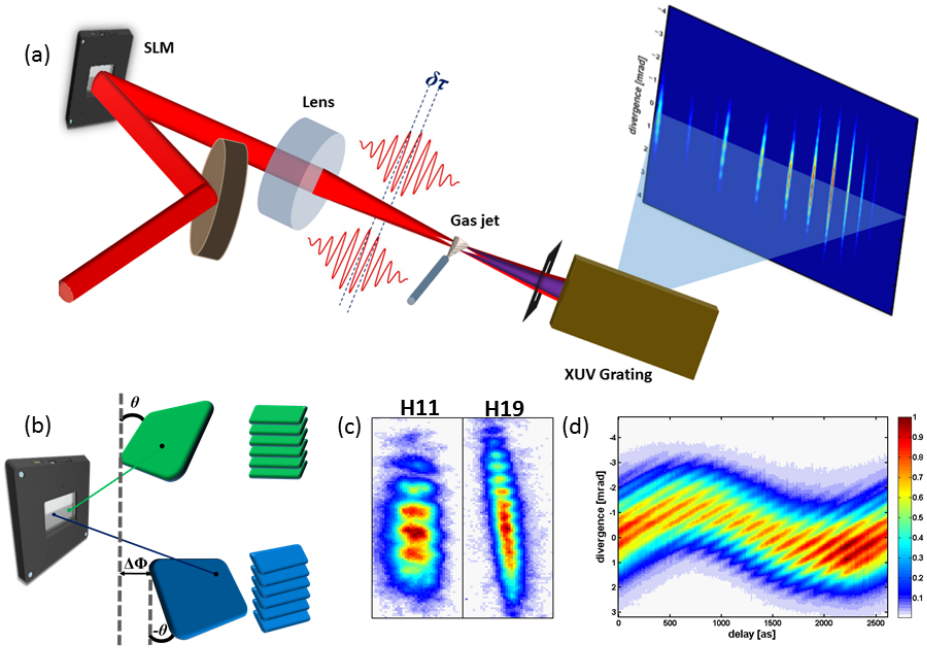

Fig. 1. (a) Experimental setup scheme. Light is reflected from an SLM and is focused into a gas jet using a lens (f=50 cm) to produce harmonics from two foci. The harmonics propagate and interfere in the far field (spectrometer detector). (b) Working schematics of the applied phase masks. The two masks are applied to the entire beam in a checkerboard pattern. The phases are wrapped in multiples of 2π. (c) Profiles of the 11th and 19th harmonic showing the interference pattern. The number of peaks changes with the wavelength (harmonic order) and with the lateral distance between the foci. (d) Evolution of the interference pattern of harmonic 11 as a function of the relative offset phase between the two masks $\Delta\Phi_{SLM}$.

optics, no relative jitter is introduced. Our technique uses similar advantages through a spatial light modulator (SLM), that allows us to reduce the necessary setup to only two optical elements; the SLM and a focusing lens. In addition, our technique relies on an elecrto-optical effect and not on mechanical stages. Further comparisons with such approaches are discussed below.

The basic idea of two-source interferometry with HHG is to generate harmonics from two identical sources or optical foci. The generated XUV pulse trains propagate in space and interfere with each other in the far field, following a pattern that closely resembles a Young's double slit interference pattern. Because the XUV radiation emitted from each source is completely coherent and has a well-defined phase relation with the driving laser, the interference pattern gives details about the phase of the quantum state of the harmonic generating medium or more precisely the phase of the induced dipole and electron wave packet.

2. Experimental setup

In this work we generate harmonics from two optical foci (f_1 and f_2) produced by a system of two-dimensional SLM and a lens (Fig. 1a)) The SLM is a Hamamatsu LCOS X10468 device. Experimentally, the device is limited by average and peak laser power in a non-trivial dependence. Usually, relevant damage threshold data can be obtained from the manufacturing company for

Optics EXPRESS

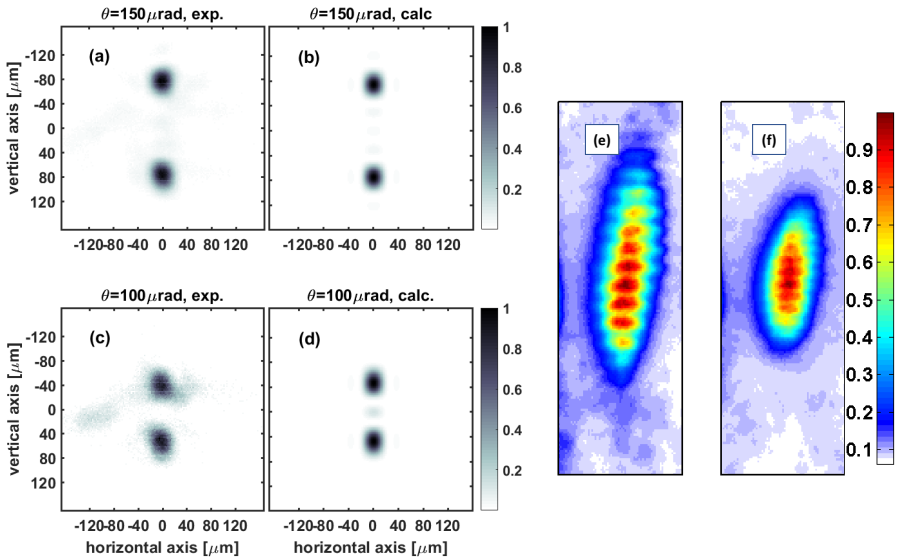

Fig. 2. Panels (a)-(d) comparison between experimental and theoretical of the two foci beam profiles at the focus with programatically controlled spot separation with the SLM. (a), experimental intensity distribution for two laser foci separated by 150μm with (b) it's theoretical simulation. (c), experimental intensity distribution for two laser foci separated by 100μm and (d) it's theoretical simulation. Panels (e) and (f) show experimental interference pattern for the 11th harmonic with separation of 120μm and 180μm respectively.

pulsed lasers. In our experiments we limit ourselves to 1.5 W of average power incident on the SLM surface at 1 kHz repetition rate and 30 fs pulses. By inserting an optical chopper, we successfully have operated the SLM with pulse energies well above 3 mJ and reduced repetition rates of 333 Hz. The SLM has an active area of 800 by 600 pixel with a surface area of 16 by 12 mm, with a diffraction/total efficiency of 75% in the experiment. The resolution or bit depth of the digital to analog converter (DAC) is 8bit, resulting in 256 possible phase steps inside the SLM, where a step of 205 is equal to 2π for 785 nm light. The two foci are generated using two alternating intertwined phase masks (Fig. 1 b) with opposite wavefront tilt. With the laser compressor we compensate for the chirp in air and glass to reach intense 30 fs (FWHM of the intensity) pulses in the interaction region to produce peak intensities at the foci of $\approx 10^{14}$W/cm^2. At these intensities, when interacting with a dense gas target, harmonics are generated at each focus. As the harmonics propagate towards the detector, they interfere in the far field. An example of the measured interference pattern of harmonics 11th (71.4 nm, 17.4 eV) and 19th (41.3 nm, 30 eV) is shown in Fig. 1c). To preserve phase matching in HHG the Rayleigh range is chosen to be much larger than the interacting region, which is 500 μm in our case. Also, the distance between the two foci, is smaller than the inner diameter of the glass capillary used to generate the gas jet and both foci generate harmonics from identical gas pressures. Practically, this means that differences in the optical path will be dictated by changes in pressures of 10^{-4} to 10^{-5} Torr over one Rayleigh range.

Similar interferometric schemes have been used in the past with HHG [20, 24, 31], but have to compromise between stability or flexibility. With our method it is possible to control the generation of the one XUV beam (spatially and temporally) independently from the other, similar to the technique in [27]. However, here everything is given by a pure electro-optical effect in the spatial light modulator, without the requirement of a stable and reliable mechanical translation

Optics EXPRESS

stage. Furthermore, our SLM approach is rather flexible when it comes to optical alignment as additional masks can be used to control the divergence of the two beams independently. By applying a voltage offset to one mask relative to thedelay or optical phase (within one cycle) of one pulse relative to the other. This is simply understood in terms of Fourier optics [32]. Since the SLM is limited in the amount of overall phase ($2.5 \times \pi$ at 785 nm), we wrap the phase similar to Fresnel lenses [32] at 2π. Because the mask is a phase change across the entire beam profile, there is only one beam with two cross wave fronts. Therefore, we are able to generate two beams that share exactly the same beam path and only become distinguishable at approximately one Rayleigh range before the focus. As the beam is focused in vacuum, the difference in optical path is only dictated by fluctuations in the background pressure over a distance of a few millimeters. Similar methods with pulse shaping have been actively used as a means of achieving zeptosecond precision interferometers [33] in a frequency domain setup, which does not allow the generation of two spatially separated pulses.

It is important to remark that the phase masks are homogeneously distributed and applied to the entire beam and not split in distinguishable halves, like in previous works [20, 34]. The phase and tilt of each pulse is identified by using two phase pattern where f_1 is controlled by “white" squares and f_2 is controlled by “black" squares. The main advantage of using an intertwined pattern is that the two beams are completely indistinguishable from each other. Compared to previous work [20, 26–28, 34], our alignment is simpler and the entire optics setup more resistant to slight beam pointing instabilities, as the alignment of the SLM is identical to the alignment of a simple mirror and there is no mechanical drift. Indeed, once calculated and applied, the SLM masks result in the expected behavior in the focus, regardless of slight misalignment. In addition, the lateral distance between the two foci (the two secondary sources) can be tuned dynamically, without any modification on the optical setup and without any realignment, only by applying on the SLM a new set of sub-patterns with a different tilt between each other. This possibility can go so far as to isolate one of the two sources. One has to just increase the tilt of one sub-pattern so much as to transpose it far away from the target. Consequently, it is possible to check the emission from each one of the two sources separately before letting them interfere in the far field. To our knowledge this is a completely new possibility in the field of HHG spectroscopy which can be utilized in order to in situ check if the two secondary sources are indeed identical.

In Fig. 2, we show experimental data and theoretical simulations for the beam characterization at the focus, with the distance between foci controlled programmatically by the SLM. Panels (a) and (c) show experimental data taken with a CCD camera at the focus. The data matches the calculations performed for identical experimental conditions in panels (b) and (d) of the figure. Smaller peaks in between, due to diffraction, are visible on the CCD as well as in the calculations. Panels (e) and (f) show experimental interference pattern for the 11th harmonic with separation of $120\mu m$ and $180\mu m$ respectively demonstrating how the fringes scale with the separation of the sources. This added flexibility shows that resolution in the interferogram can be controlled programatically with the SLM and present absolutely no mechanical drift.

It is well understood that the overall phase of the driving field has a great impact on the generation of harmonics [35]. Regarding the phase distribution, our tilted Fresnel masks produce Gaussian shaped foci with transversal phase distributions which are almost flat. When the two foci come closer than 100 μm, the two laser fields still overlap slightly at the focus and the spatial phase of the two sources is altered (through interference effects). Intensity differences of less than 1% can be observed between phase masks of altered delay. Otherwise, the phase profile across the foci is flat, except at the wings(we define wings as intensities of less than 10% of the peak intensity) for a few values of the relative phase between the two foci(e.g. $\pi/4$ and $3\pi/4$). In these cases we can observe a slight wave front tilt of the driving field which is responsible for the observed characteristic "S-shape" in Fig. 1(d).

Optics EXPRESS

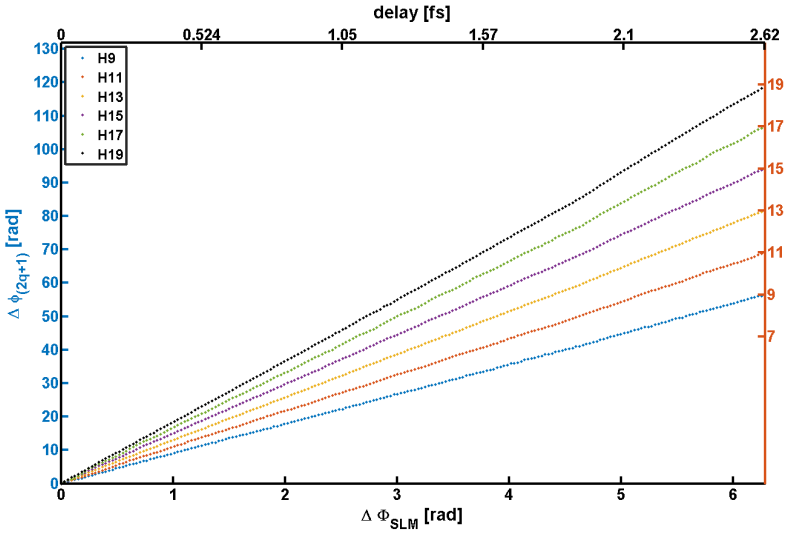

Fig. 3. Phase of harmonics 9 to 19 (left-vertical axis), measured from the interferograms as shown in Fig. 1 c), as a function of the relative SLM phase $\Delta\Phi_{SLM}$ (bottom-horizontal axis). The right axis is the phase in units of 2π showing that the phase evolution of each harmonic $2q+1$ is $\Delta\phi_{(2q+1)} = (2q+1)\times\Delta\Phi_{SLM}$. Top-horizontal axis is the corresponding delay time for a 785 nm wavelength pulse. The SLM has access to 205 phase values for 2π manipulation at 785 nm, thus capable of a resolution of 12.8 attoseconds.

3. Stability and precision measurement

We control the relative phase between the two foci by adding an offset phase to one of the tilted Fresnel masks (see Fig. 1 (b)). Since this induces a relative phase difference between the two masks at the SLM, we call it $\Delta\Phi_{SLM}$. The evolution of the interference fringes in harmonic 11 as a function of $\Delta\Phi_{SLM}$ is shown in Fig. 1 d). In our SLM we can control $\Delta\Phi_{SLM}$ with a step size of about 12.8 attoseconds at a center wavelength of 785 nm. We should point out that because the two foci are exact replicas of each other and are generated from the same driving pulse, the relative delay between the two sources is completely independent of any fluctuation of the laser. This relative delay, through the HHG process [16], is inherited to the relative phase of the harmonic fields emanating from each one of the two foci, multiplied by the order of the harmonic. Because the two foci are identical, the term of the atomic phase (which depends on the driving field intensity) [16], is the same for both of them. Consequently, it does not affect their phase difference. To more quantitatively extract the relative phase between the two harmonic sources $\Delta\phi_q$, as a function of the relative delay of the two foci we need to calculate the phase evolution for each harmonic. We can do this calculation in two ways. One option is to measure the relative displacement of the maxima and minima in the fringe pattern keeping in mind that a 2π shift corresponds to the distance between two peaks [25]. We use a second option which makes use of Fourier analysis of the fringe pattern. In this approach $\Delta\phi_q$ is the phase of the fringe frequency of the Fourier spectrum, which corresponds to the inverse spacing between peaks in the detector. Because the fringe separation in the detector is proportional to $\lambda_{(2q+1)}/D$ with D the spacing between the two sources, the fringe spacing reduces with harmonic order. For this study, we kept the separation between the two foci at $100\mu m$. The relative phase evolution for harmonics 9 to 19 (left axis) using the Frequency Fourier analysis is shown in Fig. 3. In addition, we show on the right-vertical axis the phase in units of 2π for each harmonic. From this plot the scaling of the phase $\Delta\phi_{(2q+1)}$, for each harmonic of order $2q+1$, as a function

Optics EXPRESS

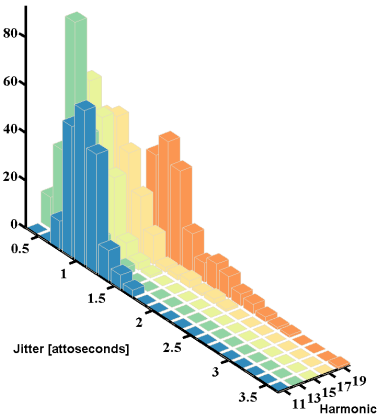

Fig. 4. Histogram of the jitter for all delays as a function of harmonic. The jitter is calculated as the standard error, for each delay value taking into account the 17 measurements done at each delay. Each of the 17 measurements are made up of 600 laser shots.

of $\Delta\Phi_{SLM}$ is clear. This scaling is another demonstration of the self-balancing geometry of our interferometer. For each oscillation period of the fundamental there are exactly $(2q + 1)$ oscillations in the electromagnetic field for harmonic $(2q + 1)$. Again, we are able to observe this thanks to the self-referencing nature of the interferometer. To be able to observe oscillations in the harmonics we need attosecond resolution in our time steps. The top-horizontal axis in Fig. 3 shows the corresponding delay time for a 785 nm center wavelength pulse. As mentioned before the SLM has a resolution of 8-bit and at 785 nm has access to 205 effective phase values over 2π, thus capable of a resolution of 12.8 attoseconds and a range of up to about 1.25 optical cycles. This resolution was confirmed by measuring the amount the fringes moved for each harmonic. However, the main limitation in most interferometers is not in the resolution but rather in the precision. Temperature, humidity and mechanical instabilities are often enough to cause errors in the orders of hundreds of attoseconds.

Table 1. **Measured precision for different harmonic orders. SE are the standard error estimates calculated from 17 images taken for each harmonic with each image consisting of 600 laser shots. HO is harmonic order.**

HO	SE [as]	Deviation [as]
9	3.10	2.8
11	0.80	0.72
13	0.68	0.60
15	0.71	0.63
17	0.80	0.71
19	1.10	0.94

To further demonstrate the precision of our method, we calculate the jitter for harmonics 9 to 19 using 17 independent experiments at each delay. The jitter is calculated from the standard

Optics EXPRESS

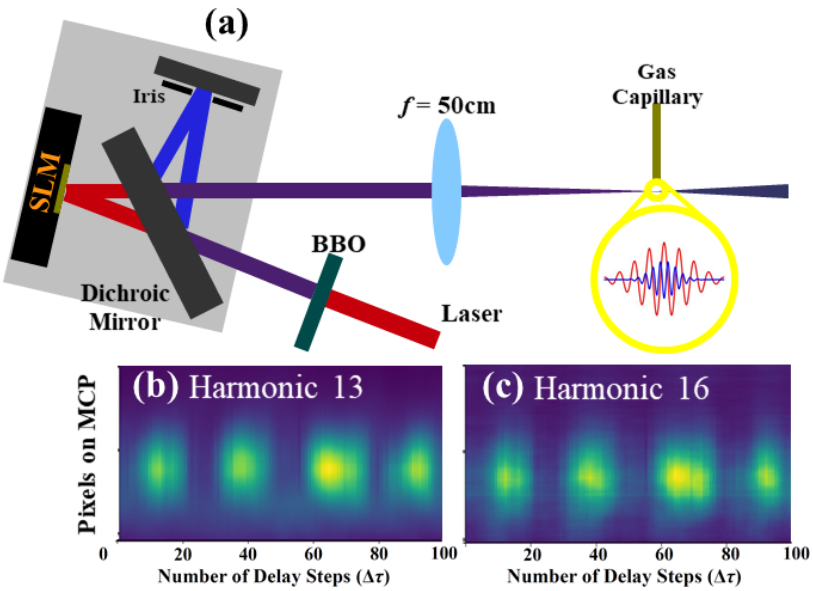

Fig. 5. (a) Experimental setup scheme for the two color interferometer. The 2nd harmonic of the 785 nm light is generated in a BBO crystal and separated by a dichroic mirror. An additional Fresnel lens mask (f = 11 m) is added to the SLM to optimize overlap between the two beams . After the recombination, 785 nm and 393 nm beams are focused together into a gas jet at a single focus. (b) and (c) Raw experimental evolution of the harmonics 13 and 16 as a function of the offset phase. The time delay step size $\delta\tau$ = 26 attoseconds.

error of the phase using the 17 measurements. Each one of the 17 measurements is comprised of 600 laser shots, the number of laser shots chosen to form a harmonic picture. Figure 4 shows the histogram of the jitter values for the 205 delay values for harmonics 11 to 19. The results, which are plotted as a histogram of the jitter values, are summarized in the Table 1. Harmonic 9 is not included in the figure but is included in the table.

The SE column reports the standard error of the jitter from the histogram and the deviation column is the standard deviation from the same distribution. From both, the histogram and the table, we can clearly observe that we have a precision better than one attosecond. Harmonic 13 has the best precision of 680 zeptoseconds followed by harmonic 15 with a precision of 710 zeptoseconds. We should mention that harmonic 9 and 19 have the worst precision of 3.1 and 1.1 attoseconds. These larger uncertainties are due to poor signal levels in harmonic 9 and due to a lack of resolution in the fringes in harmonic 19. The low signal of harmonic 9 is due to the response of the holographic grating used. As mentioned, the resolution of the fringes can be improved by changing the distance between the foci.

4. Two-color Michelson-type interferometer

In addition to the self-referencing application above, we now show that the phase delay induced can also be considered with respect to an external field. In other words, with the proposed scheme, the SLM can successfully substitute the movable arm of a Michelson-type interferometer, being able to act as a delay stage of high precision and stability. In order to support this claim, we retrieve the delay dependence on HHG when driven by a two color laser field, with polarizations perpendicular to each other, in argon gas. The results are in agreement with the already existing literature, proving the potential of the proposed technique.

Optics EXPRESS

The slightly modified experimental setup is shown in Fig. 5(a). An incoming 785 nm laser field produces its second harmonic in a 200 μm thick beta barium borate (BBO) crystal. A dichroic mirror separates the 393 nm radiation from the fundamental. The second harmonic is reflected on a flat aluminum mirror while the fundamental is reflected on the SLM surface. For better stability, the two distinct arms are built as short as possible with a length of about 4 cm each. After recombination, both the fundamental and its 2nd harmonic are focused on the gas-target by a lens with 50 cm focal length. Because of differences in the index of refraction and divergences, focusing is not the same for the two wavelengths. In order to make the two beams focus together, the fundamental beam is additionally shaped by the SLM while both are imaged on a CCD camera. An appropriate Fresnel lens pattern, corresponding to a positive focal length of 11 m, is applied on the SLM which forces the fundamental to focus closer to the lens. An intertwined pattern, as described before, is applied and the offset of one of the masks is controlled as a means of delay. In addition, we increase the tilt angle of one of the sub-patterns by one order of magnitude, obtaining a single focal spot identical to the one of the pair of spots used before. While mathematically complicated, the implementation of all these masks is very simple. All phases add and before writing to the SLM they are wrapped at a maximum value of 2π. This demonstrates the great versatility of the proposed scheme based on the use of the SLM: one is able to perform drastic adaptations to various experimental needs without changing anything in the optical setup.

For the particular two-color experiment, the compression is optimized for HHG of the fundamental, reaching a peak intensity of about 10^{14} W/cm^2. The measured duration of the 785 nm fundamental, using FROG, is 30 fs while the 2nd harmonic pulse duration is 80 fs. The polarization of the two fields are perpendicular to each other and the energy ratio of the 393 nm electric field with respect to the 785 nm electric field is 0.2. In Figs. 5(b) and 5(c), one can see the characteristic 4 yield oscillations for harmonic orders 13 and 16 for delay values spanning a full IR period; the delay step for this scan is 26 attoseconds. The four full yield oscillations behavior for an electric field amplitude ratio of 0.2 used here (which means that the 2nd harmonic field cannot be considered as just a perturbation of the fundamental) has been already confirmed experimentally [36] and explained theoretically [37, 38]. Thus, similar implementations like the recent, beautiful experiment [39], based on two-source XUV interferometry, could be even improved with our technique

5. Summary

To conclude, we have presented a novel interferometer for trains of attosecond XUV pulses generated through HHG, with tunable arms and high stability. By using an intertwined mask in a SLM we create a beam with two wavefronts that become distinguishable only in the far field. This interferometer resembles a common path homodyne detector for the fundamental laser field as two identical copies of the driving pulse are created at the focus of a simple SLM and lens optical system. Since the two beams are indistinguishable until about one Rayleigh range from the focus, their optical path are identical and almost jitter free and thus the phase between the two foci is perfectly locked. The relative phases of the driving field in each focus can be programmatically manipulated to obtain a delay resolution of 12.8 attoseconds (half of the atomic unit of time) and a precision or jitter of 0.68 attoseconds for harmonic 13 measured as the standard error. Our techniques is a different approach to the method proposed in [26, 27], capable of a similar precision, while being able to scan over a much wider temporal range. However, in our opinion, making use of eletro-optical methods allows for a better control for future sub-attosecond experiments without the use of any mechanical elements. For example, if temporal controls of 1/2 attoseconds are to be achieved in the future, mechanical control of 0.15 nm will be required. This would be equivalent to a spatial control of 10 SiO bonds in α

Optics EXPRESS

quartz. On the other hand, high bit-depth liquid crystals on silicon (LCOS) devices are already present in the market and will likely continue to improve thanks to the LCD and LED consumer markets. For example, to achieve 0.5 attosecond delay control, our method would require an LCOS-SLM with a bit depth of 13 bits, less than what is currently available in mass-produced TVs. On the other hand, some of the main limitations in SLMs are the low damage threshold and the restricted delay range. While larger LCOS devices will help with the damage threshold, they will inherently suffer from a much limited range for the delay compared to mechanical devices.

Funding

U.S. Department of Energy (DOE) (DE-FG02-86ER13491, DE-SC0019098).

References

1. E. Constant, V. D. Taranukhin, A. Stolow, and P. B. Corkum, "Methods for the measurement of the duration of high-harmonic pulses," Phys. Rev. A **56**, 3870–3878 (1997).
2. P. Paul, E. Toma, P. Breger, G. Mullot, F. Augé, P. Balcou, H. Muller, and P. Agostini, "Observation of a train of attosecond pulses from high harmonic generation," Science **292**, 1689–1692 (2001).
3. M. Hentschel, R. Kienberger, C. Spielmann, G. A. Reider, N. Milosevic, T. Brabec, P. Corkum, U. Heinzmann, M. Drescher, and F. Krausz, "Attosecond metrology." Nature **414**, 509–13 (2001).
4. J. Itatani, F. Quéré, G. L. Yudin, M. Y. Ivanov, F. Krausz, and P. B. Corkum, "Attosecond streak camera," Phys. Rev. Lett. **88**, 173903 (2002).
5. P. Tzallas, D. Charalambidis, N. Papadogiannis, K. Witte, and G. D. Tsakiris, "Direct observation of attosecond light bunching," Nature **426**, 267–271 (2003).
6. A. Baltuška, T. Udem, M. Uiberacker, M. Hentschel, E. Goulielmakis, C. Gohle, R. Holzwarth, V. Yakovlev, A. Scrinzi, T. W. Hänsch, and F. Krausz, "Attosecond control of electronic processes by intense light fields," Nature **421**, 611–615 (2003).
7. R. Kienberger, E. Goulielmakis, M. Uiberacker, A. Baltuska, V. Yakovlev, F. Bammer, A. Scrinzi, T. Westerwalbesloh, U. Kleineberg, U. Heinzmann, M. Drescher, and F. Krausz, "Atomic transient recorder," Nature **427**, 817–821 (2004).
8. G. Sansone, E. Benedetti, F. Calegari, C. Vozzi, L. Avaldi, R. Flammini, L. Poletto, P. Villoresi, C. Altucci, R. Velotta, S. Stagira, S. De Silvestri, and M. Nisoli, "Isolated Single-Cycle Attosecond Pulses," Science **314** (2006).
9. P. B. Corkum and F. Krausz, "Attosecond science," Nat. Phys. **3**, 381–387 (2007).
10. G. Kolliopoulos, P. Tzallas, B. Bergues, P. Carpeggiani, P. Heissler, H. Schröder, L. Veisz, D. Charalambidis, and G. D. Tsakiris, "Single-shot autocorrelator for extreme-ultraviolet radiation," J. Opt. Soc. Am. B **31**, 926–938 (2014).
11. M. Ossiander, F. Siegrist, V. Shirvanyan, R. Pazourek, A. Sommer, T. Latka, A. Guggenmos, S. Nagele, J. Feist, J. Burgdörfer, R. Kienberger, and M. Schultze, "Attosecond correlation dynamics," Nat. Phys. (2016).
12. S. E. Harris, J. J. Macklin, and T. W. Hänsch, "Atomic scale temporal structure inherent to high-order harmonic generation," Opt. Commun. **100**, 487–490 (1993).
13. P. Antoine, A. L' Huillier, and M. Lewenstein, "Attosecond pulse trains using high-order harmonics," Phys. Rev. Lett. **77**, 1234–1237 (1996).
14. J. L. Krause, K. J. Schafer, and K. C. Kulander, "High-order harmonic generation from atoms and ions in the high intensity regime," Phys. Rev. Lett. **68**, 3535 (1992).
15. A. L' Huillier and P. Balcou, "High-order harmonic generation in rare gases with a 1-ps 1053-nm laser," Phys. Rev. Lett. **70**, 774 (1993).
16. M. Lewenstein, P. Balcou, M. Y. Ivanov, A. L' Huillier, and P. B. Corkum, "Theory of high-harmonic generation by low-frequency laser fields," Phys. Rev. A **49**, 2117 (1994).
17. J. Itatani, J. Levesque, D. Zeidler, H. Niikura, H. Pépin, J.-C. Kieffer, P. B. Corkum, and D. M. Villeneuve, "Tomographic imaging of molecular orbitals," Nature **432**, 867–871 (2004).
18. W. Li, X. Zhou, R. Lock, S. Patchkovskii, A. Stolow, H. C. Kapteyn, and M. M. Murnane, "Time-resolved dynamics in N_2 O_4 probed using high harmonic generation," Science **322**, 1207–1211 (2008).
19. Y. Mairesse, A. de Bohan, L. J. Frasinski, H. Merdji, L. C. Dinu, P. Monchicourt, P. Breger, M. Kovačev, R. Taïeb, B. Carré, H. G. Muller, P. Agostini, and P. Salières, "Attosecond synchronization of high-harmonic soft x-rays," Science **302**, 1540–1543 (2003).
20. X. Zhou, R. Lock, W. Li, N. Wagner, M. M. Murnane, and H. C. Kapteyn, "Molecular recollision interferometry in high harmonic generation," Phys. Rev. Lett. **100**, 073902 (2008).
21. Y. Mairesse and F. Quéré, "Frequency-resolved optical gating for complete reconstruction of attosecond bursts," Phys. Rev. A **71**, 011401 (2005).
22. K. T. Kim, C. Zhang, A. D. Shiner, B. E. Schmidt, F. Légaré, D. Villeneuve, and P. Corkum, "Petahertz optical oscilloscope," Nat. Photonics **7**, 958–962 (2013).
23. A. Camper, T. Ruchon, D. Gauthier, O. Gobert, P. Salières, B. Carré, and T. Auguste, "High-harmonic phase spectroscopy using a binary diffractive optical element," Phys. Rev. A **89**, 043843 (2014).

Optics EXPRESS

24. J. Bertrand, H. Wörner, P. Salières, D. Villeneuve, and P. Corkum, "Linked attosecond phase interferometry for molecular frame measurements," Nat. Phys. **9**, 174–178 (2013).
25. R. Zerne, C. Altucci, M. Bellini, M. B. Gaarde, T. W. Hänsch, A. L' Huillier, C. Lyngå, and C.-G. Wahlström, "Phase-Locked High-Order Harmonic Sources," Phys. Rev. Lett. **79**, 1006–1009 (1997).
26. D. Brida, C. Manzoni, and G. Cerullo, "Phase-locked pulses for two-dimensional spectroscopy by a birefringent delay line," Opt. Lett. **37**, 3027–3029 (2012).
27. G. Jansen, D. Rudolf, L. Freisem, K. Eikema, and S. Witte, "Spatially resolved fourier transform spectroscopy in the extreme ultraviolet," Optica **3**, 1122–1125 (2016).
28. J. L. Ellis, K. M. Dorney, D. D. Hickstein, N. J. Brooks, C. Gentry, C. Hernández-García, D. Zusin, J. M. Shaw, Q. L. Nguyen, C. A. Mancuso *et al.*, "High harmonics with spatially varying ellipticity," Optica **5**, 479–485 (2018).
29. Y. Meng, C. Zhang, C. Marceau, A. Y. Naumov, P. Corkum, and D. Villeneuve, "Octave-spanning hyperspectral coherent diffractive imaging in the extreme ultraviolet range," Opt. Express **23**, 28960–28969 (2015).
30. D. Azoury, O. Kneller, S. Rozen, B. D. Bruner, A. Clergerie, Y. Mairesse, B. Fabre, B. Pons, N. Dudovich, and M. Krüger, "Electronic wavefunctions probed by all-optical attosecond interferometry," Nat. Photonics **13**, 54–+ (2019).
31. O. Smirnova, Y. Mairesse, S. Patchkovskii, N. Dudovich, D. Villeneuve, P. Corkum, and M. Y. Ivanov, "High harmonic interferometry of multi-electron dynamics in molecules," Nature **460**, 972–977 (2009).
32. D. G. Voelz, "Computational fourier optics: a matlab tutorial," (2011).
33. J. Köhler, M. Wollenhaupt, T. Bayer, C. Sarpe, and T. Baumert, "Zeptosecond precision pulse shaping," Opt. Express **19**, 11638–11653 (2011).
34. A. Camper, A. Ferré, N. Lin, E. Skantzakis, D. Staedter, E. English, B. Manschwetus, F. Burgy, S. Petit, D. Descamps, T. Auguste, O. Gobert, B. Carré, P. Saliéres, Y. Mairesse, and T. Ruchon, "Transverse electromagnetic mode conversion for high-harmonic self-probing spectroscopy," in "Photonics," , vol. 2 (Multidisciplinary Digital Publishing Institute, 2015), vol. 2, pp. 184–199.
35. P. Balcou, P. Salieres, A. L' Huillier, and M. Lewenstein, "Generalized phase-matching conditions for high harmonics: The role of field-gradient forces," Phys. Rev. A **55**, 3204 (1997).
36. I. J. Kim, C. M. Kim, H. T. Kim, G. H. Lee, Y. S. Lee, J. Y. Park, D. J. Cho, and C. H. Nam, "Highly efficient high-harmonic generation in an orthogonally polarized two-color laser field," Phys. Rev. Lett. **94** (2005).
37. C. M. Kim and C. H. Nam, "Selection of an electron path of high-order harmonic generation in a two-colour femtosecond laser field," J. Phys. B **39**, 3199 (2006).
38. C. M. Kim, I. J. Kim, and C. H. Nam, "Generation of a strong attosecond pulse train with an orthogonally polarized two-color laser field," Phys. Rev. A **72**, 033817 (2005).
39. P. Carpeggiani, M. Reduzzi, A. Comby, H. Ahmadi, S. Kühn, F. Calegari, M. Nisoli, F. Frassetto, L. Poletto, D. Hoff, J. Ullrich, C. D. Schröter, R. Moshammer, G. G. Paulus, and G. Sansone, "Vectorial optical field reconstruction by attosecond spatial interferometry," Nat. Photonics **11**, 383 (2017).

129.130.19.169 {ts '2019-09-13 17:00:11'}